The Geochemical Properties of the Geothermal Fluids of Northwestern Algeria: a revised conceptual framework

Mohamed Belhai [1], Brahim Ayad [1], Yasuhiro Fujimitsu [2], Rosa Maria Barragan-Reyes [3], Tatsuto Iwanaga [4], Mamiko Maeno [4], Fatima Zohra Bouchareb-Haouchine [5], Jun Nishijima [2]. Djelloul Belhai[1], Abdelhamid Haouchine[5], Abdelhafid Afalfiz[1].

[1] Laboratory of Geodynamic, Engineering Geology and Planetology LGGIP, FSTGAT, USTHB, BP 32 Al Alia, 16111, Algiers, Algeria.

[2]Department of Earth Resources Engineering, Faculty of Engineering, Kyushu University, Fukuoka, 819-0395, Japan.
[3]Universidad Michoacana de San Nicolás de Hidalgo**,** Morelia, Michoacan, Mexico.
[4]Department of Environment Kyuden Sangyo Company, Fukuoka, Japan.
[5]Laboratory of Geo-environment, Faculty of Earth Sciences, Geography and Territorial Planning, Houari Boumediene University of Sciences and Technology, BP 32 Al Alia, 16111, Algiers, Algeria.

mkhader89@gmail.com

Keywords: *Hydrothermal fluids, Northwestern Algeria, Geochemical models, Intrusive bodies, geothermometers.*

ABSTRACT

The intense tectonic activity in northwestern Algeria has given rise to Mio-Plio-Quaternary volcanism and triggered the development of numerous thermal manifestations. Two of these— Geochemical analyses of 21 thermal spring water samples reveal considerable variability in water mineralization across the region, identifying four major water types. Na^+–Cl^- and Na^+–SO_4^{2-}—are characterized by high salinity levels (up to 3794 mg/L) and elevated concentrations of F^-, B, Li^+, Br^-, and Cs, likely sourced from halite- and gypsum-rich evaporites in the surrounding lithology. The other two types—Ca^{2+}–HCO_3^- and Na^+–HCO_3^-—are linked to interactions with local carbonate formations.

Stable isotope analyses ($\delta^{18}O$ and δ^2H) suggest the waters are of fossil origin, as their significant isotopic depletion relative to modern meteoric waters cannot be fully explained by "inland" or "altitude" effects alone. These findings imply recharge under colder climatic conditions. Gas composition modeling (N_2–He1000–Ar100 vs. O_2–CO_2–He*1000) supports a meteoric origin, showing air-saturated water (ASW) signatures.

The samples are classified as 'immature', with estimated deep geothermal reservoir temperatures reaching approximately 133 °C. The updated geochemical conceptual model proposes two main flow paths for the fossil meteoric waters. (1) In the Bouhdjar geothermal zone, meteoric waters are conductively heated at depth due to high heat flow (~120 mW/m²). During their ascent through hydrothermal conduits, the fluids may be further influenced by advective heat transfer from underlying magmatic sources or by interactions with intrusive bodies. (2) In other zones, meteoric waters originate from high-altitude recharge areas of the Atlas Mountains, undergo deep circulation and heating, and may mix with cooler, Mg-rich waters or mobilize Mg^{2+} through water-rock interactions during their ascent.

1. INTRODUCTION

Geothermal development and exploration are increasing in Algeria as part of plans to diversify energy sources for electricity production, which currently relies 98% on fossil fuels. The goal is to raise the share of renewables to 40% by 2030 (Bouchareb-Haouchine, 2012; Saibi, 2015; Belhai et al., 2016a).

Northern Algeria has significant low- to medium-temperature geothermal potential, with a heat discharge of 240 MWt and an average geothermal gradient of 33 °C/km (Saibi, 2009, 2015). Many hot springs are near densely populated areas with growing demand for space heating and industrial uses.

Northern Algeria lies within the Alpine-Maghrebide belt, formed by the ongoing collision of the European and African plates since the Late Permian, through the Pangea breakup, until the early closure of the Mediterranean in the Upper Miocene (Bouaziz et al., 2002; Fourré et al., 2011; Barkaoui et al., 2014; Belhai et al., 2016a; Bouyahyaoui et al., 2017). This tectonic evolution has produced Mio-Plio-Quaternary volcanism, seismic activity, and over 120 hot springs distributed along the ~1200 km East–West Maghrebide belt. Their distribution follows fault patterns and is influenced by the underlying lithology (Saibi, 2009; Issaadi, 1992; Kedaid and Mesbah, 1996; Belhai et al., 2016b).

The Hydrothermal System of Northwestern Algeria (HSNA, Fig. 1) is divided into two main zones:

Tellian sector: includes the Occidental Tell region from the Ouarsenis Mountains and Chlef Basin to Beni Saf and Ghazaouet, with geothermal sites at Hammam Bouhdjar (BH), Hammam Bouhnifia (BHF), and Hammam Sidi Abdelly (HSB).

Atlasic foreland: south of this sector, between the Saida and Tlemcen Mountains, with sites at Hammam Rabbi (HB), Hammam Sidi Aissa (HSI), Hammam Boughrara (BGR), and Hammam Chiguer (CHGR).

The main reservoir rocks are fractured Lower Jurassic limestone and dolomite, up to 500 m thick (Belhai et al., 2016a). Thermal features include springs, sulfate precipitation zones, alteration zones, and travertine deposits, notably forming an 800 m-long, 10 m-thick structure in the BH geothermal zone (Bouyahyaoui et al., 2017). Discharged thermal waters have temperatures between 42.9 °C and 67.1 °C with artesian flow rates of 6–9 L/s (Bouchareb-

ISSN 2703-4275

Haouchine, 2012; Belhai et al., 2016a). These waters have been used since Roman times for treating pulmonary problems, arthritis, and rheumatism.

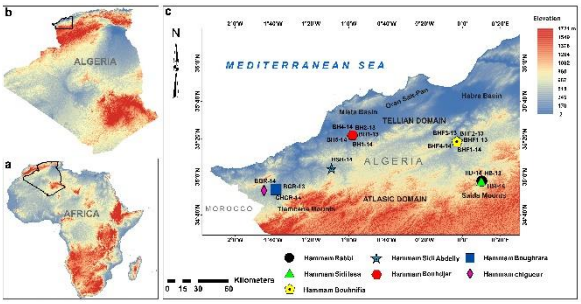

Figure 1: a) Location of Algeria in Africa, b) Location of the study area in Algeria, c) Location of hot springs in the study area.

1.1 Geology

The northernmost part of Algeria lies on the North African margin and forms the southern section of the Maghrebide Alpine belt, which extends from Gibraltar to Sicily-Calabria (Auboin and Durand-Delga, 1971; Bouaziz et al., 2002; Domzig et al., 2006; Fourré et al., 2011). The Maghrebides are divided into two main structural domains: the Tellian Atlas (Tellian) in the north and the Saharan Atlas (Atlasic foreland) in the south.

The HSNA area is situated in the external zones of the Tellian Atlas, characterized by Miocene folds and nappes that overlie the Atlasic foreland, where other HSNA sites (e.g., HB, BGR, CHGR, HSI) are located (Fig. 2a). The Tellian domain begins with coastal Paleozoic shale massifs resting on a granitic and metamorphic basement, overlain by Mesozoic clays and evaporites (Fig. 2b). This para-autochthonous Tellian substratum, of Paleozoic to Jurassic age, represents a significant geothermal reservoir (Bouyahyaoui et al., 2017).

To the south, the Habra, Mleta, and Tafna basins (Miocene–Plio-Pleistocene) contain sandstone, clay, and conglomerate formations developed during early Miocene extension. In the Mleta basin, this tectonism formed the Sebkha of Oran, a flat salt pan with a Messinian evaporite sequence deposited during the Upper Miocene closure of the Mediterranean (Aifa et al., 2003). These basins form a WSW–ENE-trending trough that separates the Paleozoic basement from the southern thrust-sheet domain (Fenet, 1975; Thomas, 1985). Volcanic intrusions (dykes, sills) occur in places such as the BGR geothermal zone of the Tafna basin (Fig. 2a), with emplacement spanning from the Miocene to the Quaternary (Maury et al., 2000; Savelli, 2002).

Further south, the Tellian thrust sheets (Sebaa Shioukh allochthonous unit) are mainly marl-sandstone with 5–10 m limestone intercalations, forming a small aquifer (Perrodon, 1957; Fenet, 1975; Megartsi, 1985; Issaadi, 1996). This nappe unit, of Vraconian to Oligocene age, is subdivided into Vracono-Senonian and Senono-Oligocene sub-units (Issaadi, 1996). These nappes were displaced southward during late Miocene compression linked to the Mediterranean closure, with shortening rates between the Iberian and Eurasian plates of ~3–6 mm/year (Belabbes et al., 2008; Nocquet and Calais, 2004; Serpelloni et al., 2007). The total thickness of the Miocene allochthonous nappes is ~250 m.

The Atlasic domain to the south is represented by the Saida and Tlemcen Mountains—a morpho-structural zone shaped by multiple Late Cretaceous tectonic phases. Structures generally trend ENE–WSW to E–W (e.g., the Horsts region in the Tlemcen Mountains) and NE–SW (e.g., the Middle Atlas and Moulouya Valley in Morocco). This domain includes Paleozoic and Jurassic formations of shale, carbonates, and dolomites, often intruded by volcanic and plutonic rocks, which are observed in the HB and HSI geothermal zones in the Saida Mountains.

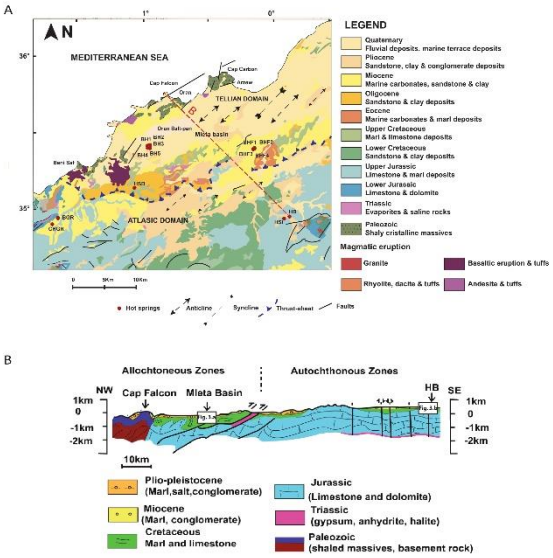

Figure 2: a) Geological map showing the different lithologies and structures of Northwestern Algeria (modified from Fenet, 1975). b) Geological cross-section through profile A-B. Red dashed lines define the location of cross-sections in the geological map.

2. WATER CHEMISTRY

The collected water samples from the two HSNA zones—(a) the Tellian sector and (b) the Atlasic foreland—show significant heterogeneity in their physicochemical features. Discharge temperatures range from 31.8 °C to 66.3 °C.

Total Dissolved Solids (TDS), calculated as the sum of major and minor ions (mg/L), are highest in zone (a), reaching up to 3794 mg/L in the Bouhdjar geothermal zone (BH). TDS decreases southward to ~443 mg/L at the HSB hot spring, farther from the Oran Salt Pan and the Mediterranean.

In zone (b), the Atlasic foreland, TDS values reach up to 2792 mg/L at the HSI hot spring, reflecting longer circulation and residence times. HSNA thermal waters have near-neutral pH values (6.1–7.5) with good correlations among salinity, pH, and chloride content, particularly in zone (a) (notably BH).

Dominant ions include Na^+ (max. 1010 mg/L), Cl^- (max. 1890 mg/L), and HCO_3^- (max. 839 mg/L). High Ca^{2+} (up to 351 mg/L) and K^+ (up to 60 mg/L) levels are also observed. Mg^{2+} content (up to 58.7 mg/L) is notably higher than in

typical high-enthalpy geothermal systems (e.g., Japan, New Zealand: 0.01–0.1 mg/L; Nicholson, 1993).

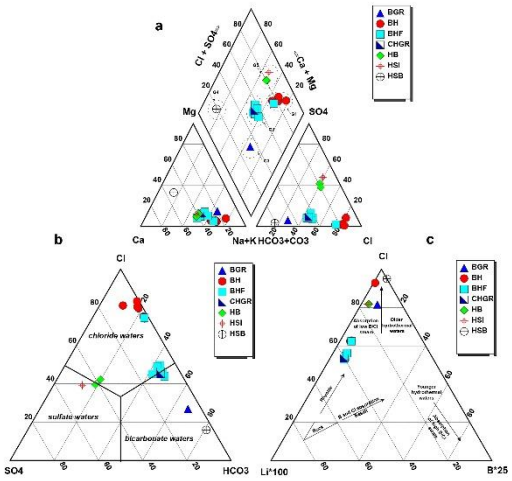

Figure 3: a) Piper diagram. b) Ternary plot (anions species), showing the wide heterogeneity in the chemistry of the collected thermal waters from Northwestern Algeria. c) Cl^--Li*100-B*25 ternary plot for the HSNA samples.

Based on TDS, EC, and pH, four water groups are distinguished:

(i) Group 1 (Na^+–Cl^-): Low-altitude BH springs (154–159 m) with TDS 1523–3794 mg/L, temperatures 41–66 °C, and pH 6.1–6.8. Cl^- is the dominant anion; Na^+ and Ca^{2+} are major cations.

(ii) Group 2 (Na^+–HCO_3^-): BHF springs (212–254 m) with TDS 1320–2142 mg/L, pH 5.94–6.59, and temperatures 42.5–66.3 °C. HCO_3^- is the main anion, with Na^+ and Ca^{2+} as cations. Tafna basin springs (BGR and CHGR) have TDS of 492–3163 mg/L, pH 6.82–7.53, and temperatures 31.8–44.8 °C.

(iii) Group 3 (Ca^{2+}–HCO_3^-): HSB spring (355 m) with TDS ~443 mg/L, pH 6.82, and temperature ~34.4 °C. HCO_3^- and Ca^{2+} dominate.

(iv) Group 4 (Na^+–SO_4^{2-}): HB and HSI springs in Saida Mountains (623–625 m) with TDS 1742–2792 mg/L, pH 6.43–6.87, and temperatures 45.5–46.2 °C. SO_4^{2-} is dominant; Na^+ and Ca^{2+} are major cations.

2.1 Minor and Trace Elements

Thermal waters generally have higher minor and trace element concentrations than cold groundwater due to increased rock–water interactions (Ma et al., 2011; Wang and Spycher, 1997; Pasvanoglu, 2013).

Arsenic (As) exceeds 10 µg/L in most HSNA samples (except CHGR, BGR, and BHF2). Notably, BHF4 has 110 µg/L, well above the WHO guideline of 10 µg/L (WHO, 1993). High As levels are likely due to interaction with sulfide-rich rocks, such as Triassic pyrite.

BH chloride waters show elevated B (1350–1680 µg/L), Li^+ (1370–1420 µg/L), Br^- (1234–1283 µg/L), and Cs (130–150 µg/L), decreasing southward in BHF bicarbonate-chloride waters (Fig. 4c). In contrast, HSB bicarbonate waters show low trace elements (e.g., B: 30 µg/L, Br^-: 133 µg/L), suggesting mixing with shallow groundwater.

Cs concentrations reflect interactions with K^+- and Mg^{2+}-rich evaporites via isomorphic substitution in minerals like sylvite and carnallite (Osichkina, 2006). This explains the low K^+ (9.97 mg/L) but high Cs (60 µg/L) in CHGR.

In the southern Atlasic domain, SO_4^{2-}-rich waters in HB and HSI show high F^- (1150–1490 µg/L). While fluoride solubility is often controlled by CaF_2, in HB and HSI it is likely sourced from biotite in nearby Paleozoic rhyolite rather than volcanic gas condensation. High F^- often coincides with elevated SO_4^{2-} and Cl^- due to proximity to rhyolitic intrusions (Fig. 4).

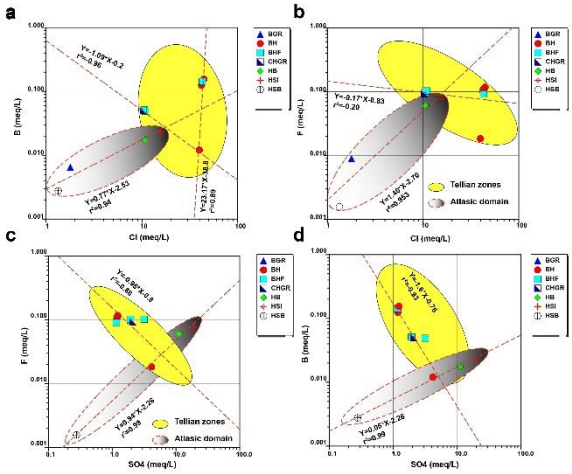

Figure 4: Scatter plots illustrating different relationships between B *vs.* Cl^- (a) F^- *vs.* Cl^- (b), F^- *vs* SO_4^{2-} (c) and B *vs* SO_4^{2-}.

3. ISOTOPIC COMPOSITION

The isotopic signatures of thermal waters help determine fluid origin and reservoir processes (Craig et al., 1956; White, 1986). δ^2H and $\delta^{18}O$ data show $\delta^{18}O$ values from −8.1 to −7.1‰ and δ^2H from −56 to −47‰ (Fig. 5a).

These values plot along the Global Meteoric Water Line (GMWL; $\delta^2H = 8.13 \times \delta^{18}O + 10.8$; Rozanski et al., 1993), indicating meteoric origin. However, their depletion compared to modern meteoric water suggests recharge during colder paleoclimatic periods, likely Pleistocene or pre-Quaternary, stored in confined aquifers—similar to northern Italy's sedimentary basins (Gorgni et al., 1982).

No significant positive $\delta^{18}O$ shift indicates minimal isotopic exchange with host rocks. Slight $\delta^{18}O$ depletion at BH1 relative to BH2 may reflect interaction with CO_2-rich fluids in the Plio-Quaternary carbonated aquifer, significant only at high temperatures.

Lower δ^2H values at higher altitudes (e.g., HB at 637 m with $\delta^2H = -56$‰; Fig. 5c) suggest recharge from higher elevations and greater distances inland. Higher Cl^- and depleted δ^2H in BH1 and BH2 indicate longer residence times and deeper circulation, characteristic of fossil reservoirs (Fig. 5b).

Tritium values in BH1 and BH2 (3.1–3.5 TU) are lower than local meteoric water (~50 TU; Issaadi, 1992), suggesting partial mixing with shallower groundwater. Generally, waters with <1 TU and high Cl^- (>500 mg/L) indicate circulation depths exceeding 50,000 years (Aksoy et al., 2009). Group 1 waters appear older than Groups 2 and 3, which show higher tritium (10–15 TU).

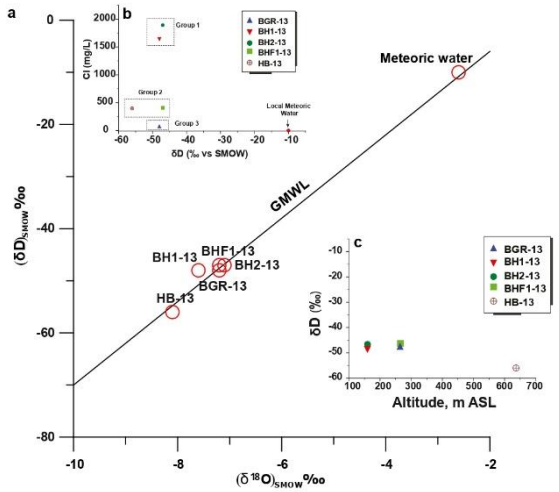

Figure 5: a) δ^2 H *vs* δ^{18} O compositions of fluids of thermal waters and local meteoric waters from Northwestern Algeria. b) Inserted plots indicate the relationship between Cl^- *vs*. δ^2 H (‰). c) Variations of δ^2 H (‰) with altitudes at spring discharge.

3.1 Gas Chemistry

Major dissolved gas compositions (N_2, O_2, CO_2, Ar, He; Table 2) show N_2-dominated samples (75.6–77.5 vol. %), moderate O_2 (18.0–20.0 vol. %), and minor Ar (0.90–0.95 vol. %), consistent with atmospheric sources (Fig. 7a).

N_2/Ar ratios (79.6–84.2) align with air-saturated water (~84), while He/Ar (2.2–4.9 × 10^{-2}) and N_2/He (1,623–3,855) ratios suggest long residence times. Elevated He likely derives from crustal sources, such as local 0.7 Ma alkali-basaltic rocks, rather than direct magmatic input.

N_2/O_2 ratios (3.77–4.22) exceed typical ASW values (~2), indicating mixing with shallow air-equilibrated waters.

In the O_2–CO_2–He diagram (Fig. 7b), moderate CO_2 enrichment (3.4–8.0 vol. %) in Tellian zone springs (BH2, BHF1) suggests additional CO_2 input from carbonate dissolution or seismic activity inducing mechano-chemical reactions (Italiano et al., 2008).

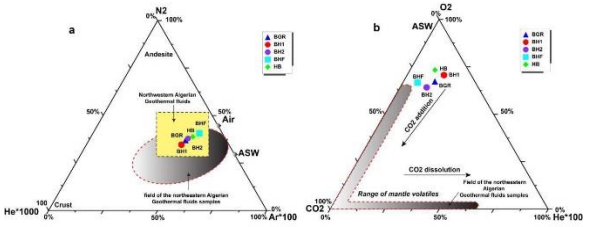

Figure 6: (a) N_2-Ar*100-He*1000 Ternary mixing model; (b) O_2-CO_2-He*100 gas mixing model for the *HSNA* thermal waters, ASW denotes Air Saturated Water.

4. CHEMICAL GEOTHERMOMETERS

Several geothermometers were used to estimate reservoir temperatures in the HSNA.

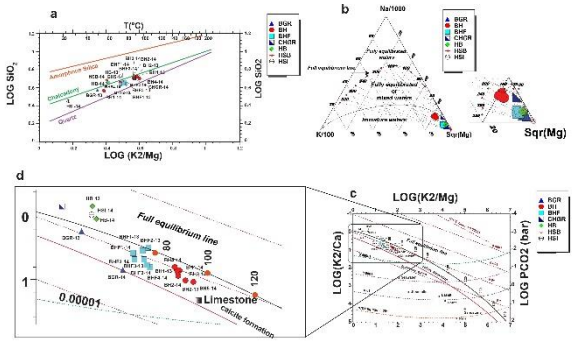

Figure 6: shows: (a) log(K^2/Mg) vs. log(SiO_2), (b) Na-K-Mg ternary diagram, (c) log(K^2/Mg) vs. log(K^2/Ca^{2+}).

As seen in Fig. 7b, many HSNA samples plot in the "immature" field near the Mg^{2+} pole, reflecting high Mg^{2+} contents from mixing with cooler, Mg-rich groundwaters. This is typical of Jurassic dolomite dissolution and indicates the fluids have not fully equilibrated. Such mixing, or cooling by boiling, reduces the reliability of cation geothermometers, which should be applied cautiously in these conditions.

The K^+/Mg^{2+} geothermometer (Giggenbach, 1988) often reflects rock dissolution rather than equilibrium, as in BGR-13 (~97 °C), but gives reasonable estimates in SO_4^{2-}-rich waters at HB (~108 °C) and HSI (~110 °C).

The silica geothermometer (Giggenbach, 1992) provides minimum reservoir temperatures, as mixing with shallow groundwater cools discharge waters, yielding values near measured temperatures.

The Na-K-Ca geothermometer (Fournier & Truesdell, 1973) tends to overestimate in Ca-rich waters (e.g. BHF4-14 ~212 °C) due to calcite dissolution, while the Na^+/K^+ geothermometer (Truesdell, 1976) often underestimates (e.g. BH1-14 ~59 °C).

More consistent estimates come from Na^+/K^+ (Fournier, 1979) at ~112 °C for BH1-14, with Na^+/K^+ (Nieva & Nieva, 1987) and K^+/Na^+ (Giggenbach, 1988) yielding broader ranges (77–136 °C) as likely maximum temperatures.

The log(K^2/Mg^{2+}) vs. log(SiO_2) diagram (Fig. 7a) shows most samples fall between chalcedony and quartz solubility curves, indicating temperatures <100 °C and control by chalcedony dissolution—typical for these mixed waters. Quartz geothermometers are less suitable here due to the limestone and dolomite reservoir lithology.

Atlasic domain samples, including HSB, plot above the chalcedony curve, indicating some variations in silica solubility control. In the BH zone, a clear mixing trend is seen from BH2-13 to BH1-14 with increasing Mg^{2+} content.

Because Mg^{2+} has inverse solubility (lower concentrations at higher temperature), Mg^{2+}-based geothermometers tend to equilibrate rapidly and can reflect shallow temperatures rather than true reservoir conditions. High Mg^{2+} content is often linked to low-temperature reservoirs.

Additionally, HSNA samples tend to plot between the "calcite formation" line and the equilibrium line with high PCO_2 values (log PCO_2 ~0.01 bar). BH thermal waters, in particular, show elevated dissolved CO_2 (up to 58.4 mg/L), which may be linked to additional CO_2 input from mantle degassing or deep-seated tectonic activity (Ristuccia et al., 2019).

5. CONCLUSION

Thermal waters from Northwestern Algeria (HSNA) show complex mineralization driven by heterogeneous lithology, tectonic setting, and hydrological processes.

HSNA waters were classified into four types: G1 (Na^+-(Ca^{2+})-Cl^--(HCO_3^-)), G2 (Na^+-HCO_3^-), G3 (Ca^{2+}-HCO_3^-), and G4 (Na^+-SO_4^{2-}). G1 and G4 chemistries reflect evaporite influence, while G2 and G3 are controlled by calcite-bearing rocks.

In G1 (BH) waters, magmatic rock weathering dominates. Origins include brine–seawater mixing (G1) and marine sediment interaction (G2).

Waters are generally immature, with mixing of high-Mg^{2+} groundwater. Reservoir temperatures reach up to ~133 °C.

Gas analyses confirm meteoric origins.

Stable isotopes also indicate meteoric recharge, with isotopic depletion suggesting infiltration under cooler, wetter paleoclimates; altitude effects are evident in HB springs.

Waters result from mixing hot deep fluids (PGL1/PGL2) with cooler Mio-Plio-Quaternary aquifer waters, with hot fractions between ~25–59%.

An updated conceptual model is proposed to aid future resource development.

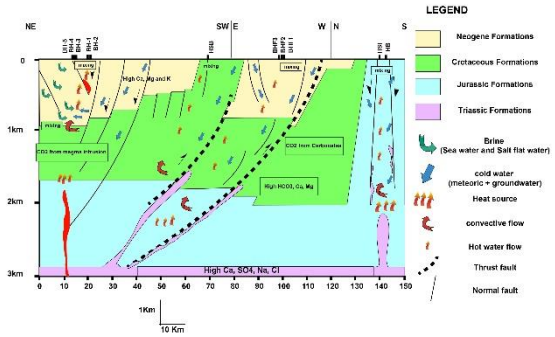

Figure 8: Conceptual evolution model of thermal waters within the hydrothermal system of Northwestern Algeria.

ACKNOWLEDGEMENTS

We sincerely thank MEXT (Ministry of Education, Culture, Sports, Science and Technology, Japan), the G-COE program, and the Laboratory of Geothermics at Kyushu University for funding this research. We also thank the Department of Environment of Kyuden Sangyo Co., Inc. (Japan).

REFERENCES

Aïfa, T., Feinberg, H., Derder, M.E., and Merabet, N.E. (2003). Contraintes magnétostratigraphiques concernant la durée de l'interruption des communications marines en Méditerranée occidentale pendant le Messinien supérieur. Geodiversitas, 25, 617-631.

Aksoy, N., Simsek, S., Gunduz, O. (2009). Groundwater contamination mechanism in a geothermal field: a case study of Balçova Turkey. J Contam Hydrol, 103, 13–28.

Auboin, J., and Durand-Delga, M. (1971). Aire méditerranéenne. Encyclopidia Universalis, 10, 743–745.

Barkaoui, A.E., Zarhloule, Y., Rimi, A., Verdoya, M., Bouri, S. (2014). Hydrogeochemical investigations of thermal waters in the northeastern part of Morocco. Environ Earth Sci, 71, 1767–1780.

Belabbes, S., Meghraoui, M., Cakir, Z., and Bouhadad, Y. (2008). InSAR analysis of a blind thrust rupture and related active folding: the 1999 Ain Temouchent earthquake (Mw5.7, Algeria) case study. J Seismol, 13, 421-432.

Belhai, M., Fujimitsu, Y., Bouchareb-Haouchine, F.Z., Iwanaga, T., Nishijima, J. (2016a). Hydrogeochemical and isotope geochemical study of northwestern Algerian thermal waters. Arab J Geosci, 9(3), 169.

Belhai, M., Fujimitsu, Y., Bouchareb-Haouchine, F.Z., Haouchine, A., Nishijima, J. (2016b). A hydrochemical study of the Hammam Righa geothermal waters in north-central Algeria. Acta Geochim, 35(3), 271–287.

Bouchareb-Haouchine, F.Z. (2012). Etude Hydrochimique des Sources Thermales de l'Algérie du Nord - Potentialités Géothermiques. Thèse Doctorat Es Science, USTHB, Algiers, 135 p.

Bouaziz, S., Barrier, E., Soussi, M., Turki, M., and Zouari, H. (2002). Tectonic evolution of the northern African margin in Tunisia from paleo stress data and sedimentary record. Tectonophysics, 357, 227–253.

Bouyahyaoui, B., Abtout, A., Hamai, L., Boukerbout, H., Djellit, H., Bougchiche, S.S., Bendali, M., Bouabdallah, H. (2017). Structural Architecture of the Hydrothermal System from Geophysical Data in Hammam Bouhadjar Area (Northwest of Algeria). Pure Appl. Geophys., 174, 1471–1488.

Craig, H., Boato, G., White, D.E. (1956). Isotopic geochemistry of thermal waters. National Acad. Sci. National Research Council Publication, 400, 29-38.

Domzig, A., Yelles, A-K., Le Roy, C., Déverchère, J., Bouillin, J-P., Bracene, R., Mercier de Lépinay, B., Le Roy, P., Calais, E., Kherroubi, A., Gaullier, V., Savoye, B., and Pauc, H. (2006). Searching for the Africa–Eurasia Miocene boundary offshore western Algeria (MARADJA'03 cruise). C R Geosci, 338, 80–91.

Fenet, B. (1975). Recherche sur l'Alpinisation de la Bordure Septentrionale du Bouclier Africain à Partir de l'Etude d'un Elément de l'Orogenèse Nord Maghrébine, Les Monts du Djebel Tessala et les Massifs du Littoral Oranais. Thèse de Doctorat d'Etat.

Fourré, E., Di Napoli, R., Aiuppa, A., Parello, F., Gaubi, E., Jean-Baptiste, P., Allard, P., Calabrese, S., and Ben Mamou, A. (2011). Regional variations in the chemical and helium–carbon isotope composition of geothermal fluids across Tunisia. Chem Geol, 288, 67–85.

Fournier, R.O. (1979). A revised equation for Na/K geothermometer. Geoth Res Council Trans, 3, 221-224.

Fournier, R.O., and Truesdell, A.H. (1973).An empirical Na–K–Ca geothermometer for natural waters. Geochimica et Cosmochimica Acta, 37, 1255-1275.

Giggenbach, W.F. (1988). Geothermal solute equilibria. Derivation of Na-K-Mg-Ca geoindicators. Geochimica et Cosmochimica Acta, 52, 2749–2765.

Giggenbach, W.F. (1992). Isotopic composition of geothermal water and steam discharges. In: D'Amore, F. (Coordinator), Application of Geochemistry in Geothermal Reservoir Development, UNITAR/UNDP, Vial del Corso, Italy, 253–273.

Gorgoni, C., Martinelli, G., Sighinolfi, G.P. (1982). Isotopic evidence of paleowaters in the Po sedimentary basin (Northern Italy). Chemical Geology, 16(2), 51-61.

Issaadi, A. (1992). Le Thermalisme dans son Cadre Geostructural, Apport à la connaissance de la structure profonde de l'Algérie et de ses Ressources Géothermales. Thèse Doctorat d'Etat, Univ. Sci. et Tech, Alger.

Issaadi, A. (1996). Mécanismes de fonctionnement des systèmes hydrothermaux. Application aux eaux thermo-minérales algériennes et aux eaux de Hammam Bou-Hadjar. Bulletin du Service Géologique de l'Algérie, 7(1), 71–85.

Italiano, F., Martinelli, G., Plescia, P. (2008). CO2 degassing over seismic areas: the role of mechanochemical production at the study case of Central Apennines. Pageoph, 165.

Kedaid, F-Z., Mesbah, M. (1996). Geochemical approach to the BouHadjar hydrothermal system (NE Algeria). Geothermics, 25, 249–257.

Ma, R., Wang, Y., Sun, Z., Zheng, C., Ma, T., and Prommer, H. (2011). Geochemical evolution of groundwater in carbonate aquifers in Taiyuan northern China. Appl. Geochem., 26, 884–897.

Maury, R.C., Fourcade, S., Coulon, C., El Azzouzi, M., Bellon, H., Coutelle, A. (2000). Post-collision neogene magmatism of the Mediterranean Maghreb margin: a consequence of slab breakoff. Comptes Rendus de l'Académie des Sciences Paris, 331, 159–173.

Megartsi, M. (1985). Le volcanisme mio-plio-quaternaire de l'Oranie Nord occidentale. Thèse Doc. Etat, U.S.T.H.B, Alger, 296 p.

Nieva, D., and Nieva, R. (1987). Development in geothermal energy in Mexico, part 12—a cationic composition geothermometer for prospection of geothermal resources. Heat Recover Syst, CHP 7, 243–258.

Nicholson, K.N. (1993). Geothermal fluids. Chemistry and exploration techniques, xv + 263 p.

Nocquet, J.M., and Calais, E. (2004). Geodetic measurements of crustal deformation in the western Mediterranean and Europe. Pure Appl. Geophys., 161, 661-681.

Osichkina, R.G. (2006). Regularities of trace element distribution in water-salt systems as indicators of the genesis of potassium salt rocks: an example from the Upper Jurassic Halogen Formation of Central Asia. Geochem Int, 44, 164–174.

Pasvanoğlu, S. (2013). Hydrogeochemistry of thermal and mineralized waters in the Diyadin (Ağri) area Eastern Turkey. Appl. Geochem., 38, 70–81.

Perrodon, A. (1957). Etude géologique des bassins néogènes sublittoraux de l'Algérie occidentale. Service de la Carte Géologique de l'Algérie (Nouvelle Série), Bulletin N° 12, 368 p.

Ristuccia, G., Bonfanti, P., Giammanco, S., Stella, G. (2019). Assessment of the Geochemical Potential in a Complex Tectonic Environment of South-East Sicily: New insights From Hydrochemical Data. Frontier in Earth Sciences, 7, 88, 1–13.

Rozanski, K., Araguás-Araguás, L., and Gonfiantini, R. (1993). Isotopic patterns in modern global precipitation. In: Swart, P.K. (ed), Climate Change in Continental Isotopic Records, American Geophysical Union Monogr. Ser., 78, Washington, DC, USA, 1–36.

Saibi, H. (2009). Geothermal resources in Algeria. Renew Sust Energ Rev, 13, 2544–2552.

Saibi, H. (2015). Geothermal resources in Algeria. Proceedings of the World Geothermal Congress, Melbourne, Australia.

Savelli, C. (2002). Time-space distribution of magmatic activity in the western Mediterranean and peripheral orogens during the past 30 Ma (a stimulus to geodynamic considerations). Journal of Geodynamics, 34(1), 99–126.

Serpelloni, E., Vannucci, G., Pondrelli, S., Argnani, A., Casula, G., and Anzidei, M. (2007). Kinematics of the western Africa Eurasia plate boundary from focal mechanisms and GPS data. Geophys J Int, 169, 1180-1200.

Thomas, G. (1985). Géodynamique d'un bassin intramontagneux; le bassin du bas Cheliff occidental (Algérie) durant le Mioplioquaternaire. Ph.D. Thesis, Université de Pau et Pays de l'Adour, France.

Wang, Y., and Spycher, G.M. (1997). Genesis of thermal groundwaters from Siping'an district, China. Appl. Geochem., 12, 437–445.

White, A.F. (1986). Chemical and isotopic characteristics of fluids within the Baca Geothermal Reservoir, Valles Caldera, New Mexico. J Geophys Res, 91, 1855–1866.